

Article

# Martensite Transformation and Mechanical Properties of Polycrystalline Co-Ni-Al Alloys with Gd Doping

Jia Ju <sup>1,2,3,\*</sup>, Huan Liu <sup>4</sup> , Ligu Shuai <sup>2,\*</sup>, Zhuang Liu <sup>1</sup>, Yan Kang <sup>1</sup>, Chen Yan <sup>5</sup> and Hong Li <sup>6</sup>

<sup>1</sup> Jiangsu Key Laboratory of Advanced Structural Materials and Application Technology, School of Materials Engineering, Nanjing Institute of Technology, Nanjing 211167, China; liuzhuang114@126.com (Z.L.); kangyan114@126.com (Y.K.)

<sup>2</sup> School of Mechanical Engineering, Southeast University, Nanjing 211189, China

<sup>3</sup> Hangzhou Kaiërda Electric Welder CO., Ltd., Hangzhou 310000, China

<sup>4</sup> College of Mechanics and Materials, Hohai University, Nanjing 211100, China; liuhuanseu@hhu.edu.cn

<sup>5</sup> Zhongtian Alloy Technology CO., Ltd., Nantong 226010, China; yanchen@chinaztt.com

<sup>6</sup> Faculty of Mechanical and Material Engineering, Huaiyin Institute of Technology, Huaian 223003, China; jnwslhong@163.com

\* Correspondence: materialju@njit.edu.cn (J.J.); shuailiguo114@126.com (L.S.); Tel.: +86-181-5100-7171 (J.J.)

Received: 2 October 2018; Accepted: 17 October 2018; Published: 18 October 2018



**Abstract:** In order to improve the mechanical properties and phase transition temperature, the influence of Gd doping on the microstructure, phase transition temperature and mechanical properties of Co<sub>35</sub>Ni<sub>32</sub>Al<sub>33</sub> alloy was investigated. The results show that the  $\gamma+\beta$  phase was observed in the microstructure of the sample with less Gd doping and the  $\gamma$  phase+martensite was found with more Gd content. The phase transition temperature apparently increases with Gd doping and the phase transition temperature goes over room temperature when the Gd is 3 at.% or more. With increasing Gd doping, more  $\gamma$  phase appears in the sample which results in decrease in hardness. The compressive strength decreases from 2274 to 1630 MPa and the ductility increase from 4.2 to 12.9% with increasing Gd content.

**Keywords:** Co-Ni-Al alloy; ferromagnetic shape memory alloy; martensite transition; mechanical properties; Gd

## 1. Introduction

Since the first observation of the magnetic field induced strain in Ni<sub>2</sub>MnGa by Ullakko [1], the ferromagnetic shape memory alloys (FSMAs) have attracted a great attention as a kinds of intelligent material for actuator and sensor. In past two decades, based on twin martensite variants remigration, numerous FSMAs, such as Ni-Mn-Ga [2–4], Co-Ni-Al [5,6], Mn-Ni-Sn [7], and Ni-Fe-Ga [8,9], achieved 8–10% giant stain. However, the actuator and sensor made of FSMAs did not get a wide range of applications due to their low phase transition temperature and poor mechanical properties [10].

In the FSMAs family, Co-Ni-Al alloy, as a potential material for actuators and sensors, can overcome the low phase transition temperature and poor mechanical properties barriers depending on their microstructures and wide range phase transition temperature [11]. In the Co-Ni-Al ternary phase diagram, a wide composition range of dual-phases ( $\gamma$  phase+ $\beta$  phase or  $\gamma$  phase+martensite) structure is obtained [6,12]. However, the microstructure of the  $\beta$  phase (B2 body-centered cubic structure) and martensite (L1<sub>0</sub> tetragonal structure) is extremely brittle, but the presence of the  $\gamma$  phase (A1 disordered face-centered cubic structure) can greatly improve ductility of the alloy. Meanwhile, the phase transition temperature of Co-Ni-Al is sensitive to material composition, especially magnetic elements [13–15]. In this case, the Co-Ni-Al alloy with excellent

mechanical properties and high phase transition temperature can be achieved by microstructure and magnetic elements modulation [6,16,17].

In previous studies, the martensite transformation process in Ti [18–20] and Fe [21] alloys had been clear, but in Co-Ni-Al FSMAs, a low martensite transformation temperature has still restricted its industrial applications. For another, doping magnetic rare elements in FSMAs, i.e., Dy [16,22], Tb [23], Nd [24], or Gd [25,26], can significantly affect the microstructure variation and phase transition temperature. Among those doping elements, the 3d electrons in rare earth Gd are delocalized and exterior, escorting to promote the valence electron concentration ( $R_{e/a}$ ) and the magnetic valence number ( $Z_m$ ) of alloys [25]. However, the effect of mechanical properties and phase transition temperature with Gd doping in Co-Ni-Al alloy is still lacking. In order to improve the mechanical properties and phase transition temperature, different amount of Gd was doped in  $\text{Co}_{35}\text{Ni}_{32}\text{Al}_{33}$  FSMAs. Thus, the influence of Gd content on the microstructure, phase transition temperature and mechanical properties of  $\text{Co}_{35}\text{Ni}_{32}\text{Al}_{33}$  alloy was aimed at in this work.

## 2. Materials and Methods

The alloy with a nominal composition of  $\text{Co}_{35}\text{Ni}_{32}\text{Al}_{33-x}\text{Gd}_x$  ( $x = 0, 1, 3, 5$ ) were prepared using high purity cobalt, nickel, aluminum and gadolinium (>99.99 at.%) in melting furnace with argon atmosphere. In order to ensure homogeneity, the sample was melted four times, then annealed at 1473 K for 3 h and quenched into ice water.

In order to determine the multiple phases of sample, X-ray diffraction (XRD, Philips PW170, Amsterdam, The Netherlands) using  $\text{CuK}\alpha$  radiation source was employed in the range of  $10\text{--}90^\circ$  at room temperature (about 300 K). the martensitic transformation temperature of the sample were analyzed by differential scanning calorimeter (DSC, STA449 F3, Netzsch, Selb, Germany) with the cooling and heating rate of 5 K/min. The structure of martensitic phase was identified using transmission electron microscopy (TEM, JOEL 2000EX, Tokyo, Japan) with selected area electron diffraction (SAED) analysis. The sample for TEM test was thinned by twin jet electro-polishing with a solution of 5% perchloric acid and 95% ethanol. The hardness of the sample was measured using Vickers hardness tester with load of 20 N. The compression tests with sample size 5 mm (length)  $\times$  3 mm width)  $\times$  3 mm (thickness) were performed on a CMT5105 (MTS, Shenzhen, China) electronic universal testing machine at the cross-head displacement speed of 0.05 mm/min. The volume fraction of  $\gamma$  phases was determined by means of the image analyzer.

## 3. Results

### 3.1. Effect of Martensite Transition on Ga Doping

#### 3.1.1. Martensite Structure

As is well known, the magnetic field induced strain of MSMA depend on twin martensite boundary migration, therefore, the martensite with twin structure plays a major role. Figure 1 shows the XRD patterns of the sample with Gd doping at room temperature. It is clear, the major peaks of the sample without Gd doping ( $x = 0$ ) and the sample with a small amount of Gd doping ( $x = 1$ ) are identified to be B2 type austenite ( $\beta$  phase) and A1 type second phase ( $\gamma$  phase). The appearance of austenite indicated that the  $M_s$  is below the room temperature. In contrast, the diffraction peaks of the sample with further doping ( $x = 3$  and 5) are correspond to  $L1_0$  type martensite and A1 type  $\gamma$  phase mixture. The lattice parameter of martensite is found to be  $a = 0.3819$  nm,  $c = 0.3124$  nm and  $c/a = 0.8153$  ( $x = 3$ ) and  $a = 0.3817$  nm,  $c = 0.3156$  nm and  $c/a = 0.8268$  ( $x = 5$ ). The increasing of  $c/a$  value indicates that the martensite unit cell increases when Gd is doped. Moreover, the diffracted intensity of martensite becomes stronger with increasing Gd content from 3 at.% to 5 at.%. The appearance of martensite in XRD patterns suggests that the sample with further doping ( $x = 3$  and 5) undergoes

martensitic transformation from B2 type austenite ( $\beta$  phase) to  $L1_0$  type martensite at room temperature. This result is in a good agreement with the DSC analysis.

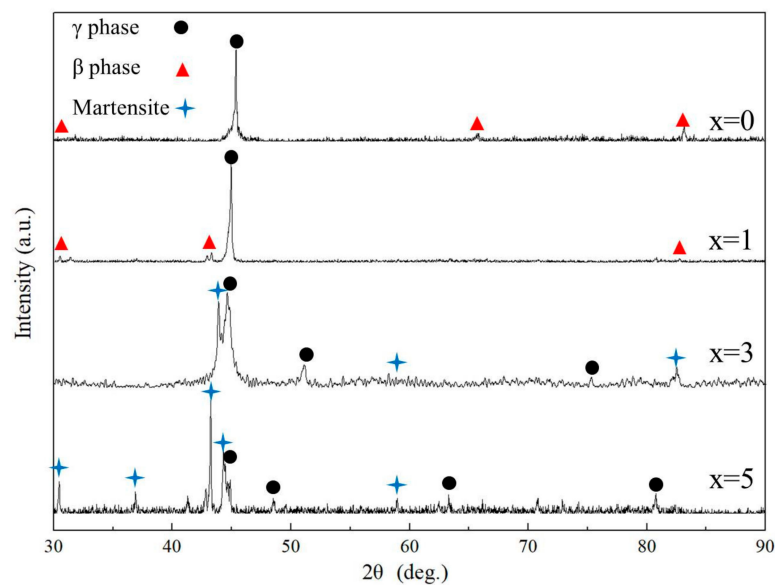


**Figure 1.** The XRD patterns of the sample with Gd doping at room temperature.

In order to further confirm the structure of martensite, TEM micrographs and selected area diffraction patterns (SADPs) of martensite of the sample with 3 at.% Gd doping ( $x = 3$ ) in Figure 2 are analyzed. It can be seen that the morphology of martensite consists of uniform black and white stripes alternatively and parallel to each other at approximately  $45^\circ$ , indicating that the martensite possesses a typical twin structure. Furthermore, the SADPs of martensite in Figure 2b along  $[001]$  zone axis shows that the diffraction spots belong to the  $L1_0$  twin structure with the  $(\bar{1}\bar{1}1)$  twinning plane.

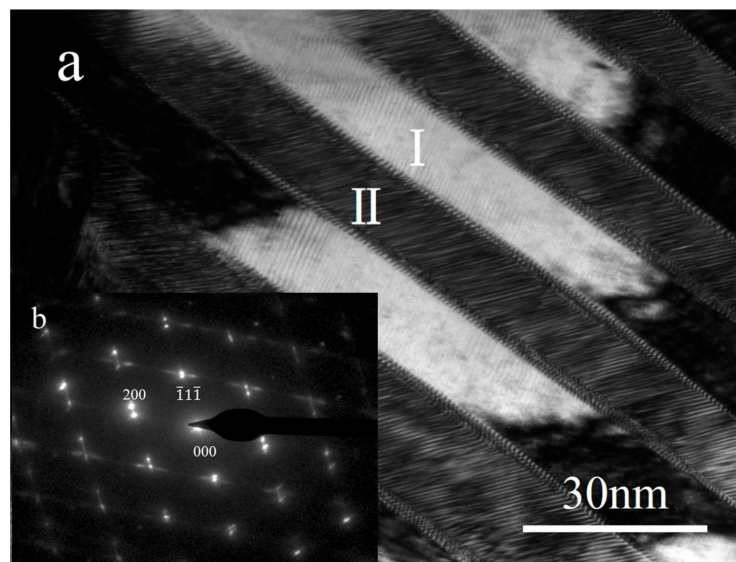


**Figure 2.** Martensite structure in a TEM micrograph (a) and the corresponding selected area electron diffraction patterns (b).

### 3.1.2. Martensitic Transformation Temperature on Gd Doping

Generally, the application temperature of MSMA (i.e., Co-Ni-Al series) based on twin martensite boundary migration depends on the stable temperature of martensite. Therefore, it is necessary to promote the martensitic transformation temperature and broaden the stable temperature range

of martensite. The martensitic transformation temperature (including the martensitic transformation start ( $M_s$ ) or finish ( $M_f$ ) temperature and the austenite transformation start ( $A_s$ ) or finish ( $A_f$ ) temperature) of samples with Gd doping between 200~400 K were analyzed using the DSC test and the result is shown in Figure 3. From DSC curves (Figure 3a), only one endothermic and one exothermic peak is observed during heating and cooling processes, which is a typical characteristic of one-step phase transformation as temperature fluctuates. In Figure 3b, the phase transformation temperature of the sample without Gd doping ( $x = 0$ ) is found to be at room temperature ( $M_s = 231$  K,  $M_f = 209$  K,  $A_s = 234$  K and  $A_f = 263$  K). When a small amount of Gd is doped ( $x = 1$ ), the phase transformation temperature increases apparently, especially the  $M_s$  and  $A_f$  increase amplitude by more than 25 K (the  $M_s$  rises from 231 K to 257 K and the  $A_f$  rises from 263 K to 296 K). Compared, the  $M_f$  and  $A_s$  had slightly increase amplitude (about 20 K, the  $M_f$  rises from 209 K to 224 K and the  $A_s$  rises from 234 K to 256 K). With increasing doping content ( $x = 3$ ), the phase transformation temperature shows a clear increasing tendency, e.g.,  $M_s$  rises to 337 K,  $M_f$  rises to 299 K,  $A_s$  rises to 320 K, and  $A_f$  rises to 357 K. For further doping ( $x = 5$ ), the tendency of phase transformation temperature increasing gradually flattened, e.g.,  $M_s$ ,  $M_f$ ,  $A_s$  and  $A_f$  rises to 373 K, 339 K, 355 K and 391 K, respectively.

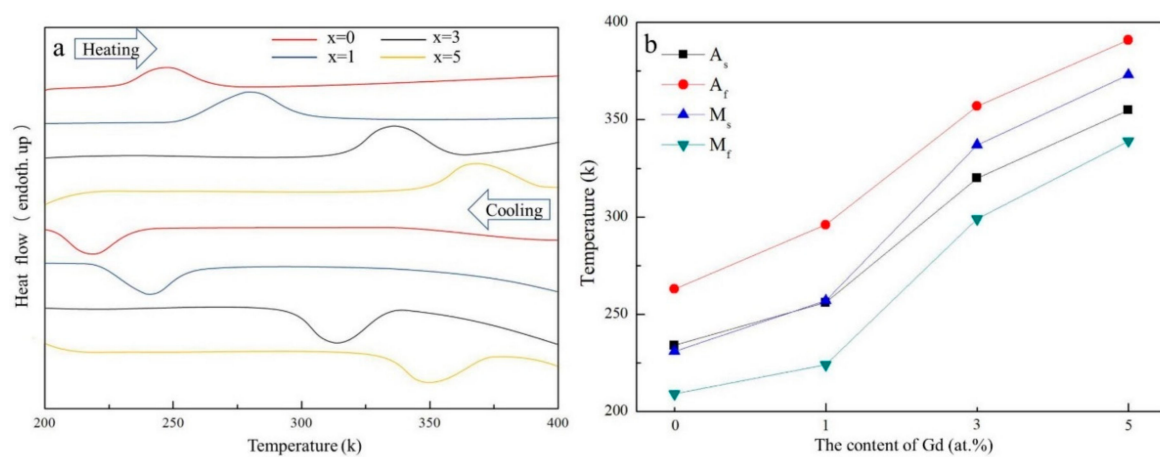


**Figure 3.** DSC curves of samples with Gd doping (a) and the martensitic transformation temperature of the sample with Gd doping (b).

### 3.1.3. Discussions on Martensite Transition with Ga Doping

It is clear that the martensitic transformation temperature of samples rapidly increases for  $x = 1$  and 3, followed by slow increase when  $x = 5$ . In fact, the martensitic transformation temperature is very sensitive to the change of the  $R_{e/a}$  of MSMA and a linear increasing correlation between  $R_{e/a}$  and  $M_s$  can be analyzed using Equation (1) for other MSMA system [3]:

$$M_s/10,000 = -1.478 + 0.1933 \times R_{e/a} - 0.1643 \times Z_m \quad (1)$$

where  $M_s$  is the martensitic transformation start temperature and  $Z_m$  is the magnetic valence number of the alloy. Figure 4 shows the relationship between  $R_{e/a}$  and the martensitic transformation temperature in the sample with Gd doping. Whereas, the  $R_{e/a}$  value can be evaluated by Equation (2) [19]:

$$R_{e/a} = \sum (X_i \times Y_i) \quad (2)$$

where  $X_i$  is the atomic valence electron of element  $i$  and  $Y_i$  is the proportion of element  $i$ . For alloys, the atomic valence electron of Co, Ni, Al, and Gd is 9 (core+3d<sup>7</sup>4s<sup>2</sup>), 10 (core+3d<sup>8</sup>4s<sup>2</sup>), 3 (core+3s<sup>2</sup>3p<sup>1</sup>), and 10 (core+4f<sup>7</sup>5d<sup>1</sup>6s<sup>2</sup>), respectively. From Figure 4, it is obvious that the relationship between

$R_{e/a}$  and the  $M_s$  is non-linear. The new relationship between  $R_{e/a}$  and  $M_s$  can be described using the following Equation (3) [12]:

$$M_s = 0.2571 R_{e/a}^2 + 0.1933 \times R_{e/a} + 0.1933 \quad (3)$$

Clearly, the curve is divided into two parts based on different slope in Figure 4. Part 1: when the  $R_{e/a}$  value is below 7.55, the  $M_s$  shows a clear rising trend. Part 2: when the  $R_{e/a}$  value is greater than 7.55, the increasing trend of  $M_s$  becomes slow. This nonlinear relationship between the  $R_{e/a}$  and the  $M_s$  is similar to the study of Rekik [7]. The reason for this phenomenon can be attributed to the size effect of doping element. Due to great difference atomic radius between Al (0.182 nm) and Gd (0.254 nm), the volume of the unit cell of sample increases when Gd substitutes Al (as XRD observations), therefore, the relative position changes of the Brillouin zone boundary and Fermi surfaces occur, which results in a slow down of the  $M_s$  increasing trend [6]. At the beginning of doping, a small amount of Gd-substituted Al and the size effect is too weak to inhibit the  $M_s$  increase. However, with further doping, the alloy displays a stronger size effect and inhibits the  $M_s$  increase clearly.

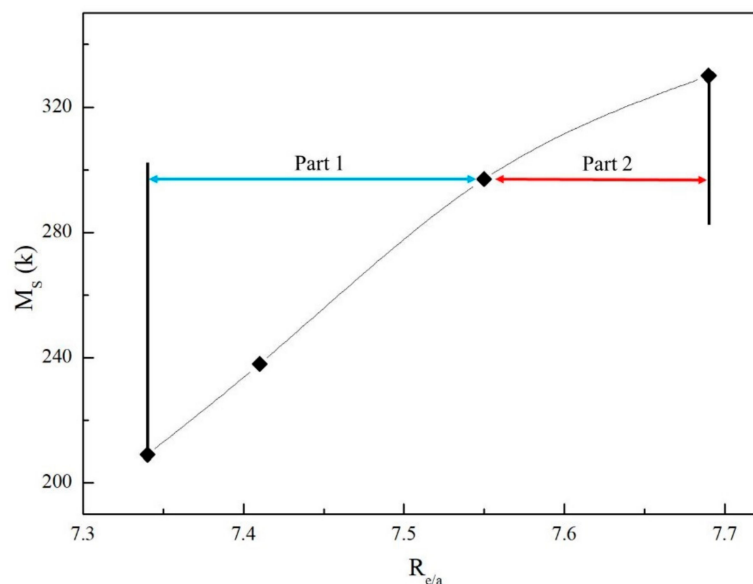


**Figure 4.** The relation between  $R_{e/a}$  and  $M_s$  of the sample with Gd doping.

### 3.2. Effect of Ga Doping on Mechanical Properties

#### 3.2.1. Effect of Ga Doping on Hardness

The HV2 (20 N as load) of the sample with Gd doping was shown in Figure 5. The Vickers hardness shows an “snake”-like decreases trend with Gd doping, i.e., the Vickers hardness value is 396, 356, 265 and 253 when Gd doping content is 0 at.%, 1 at.%, 3 at.%, and 5 at.%, respectively. According to the different decline trend, the hardness curves can be divided into three levels. (1) The first level: the hardness represents a slow decreasing trend when  $x = 1$ ; (2) the second level: the hardness displays a rapid decreasing trend when  $x = 3$ ; (3) the third level: the hardness shows a slow decreasing trend again when  $x = 5$ .

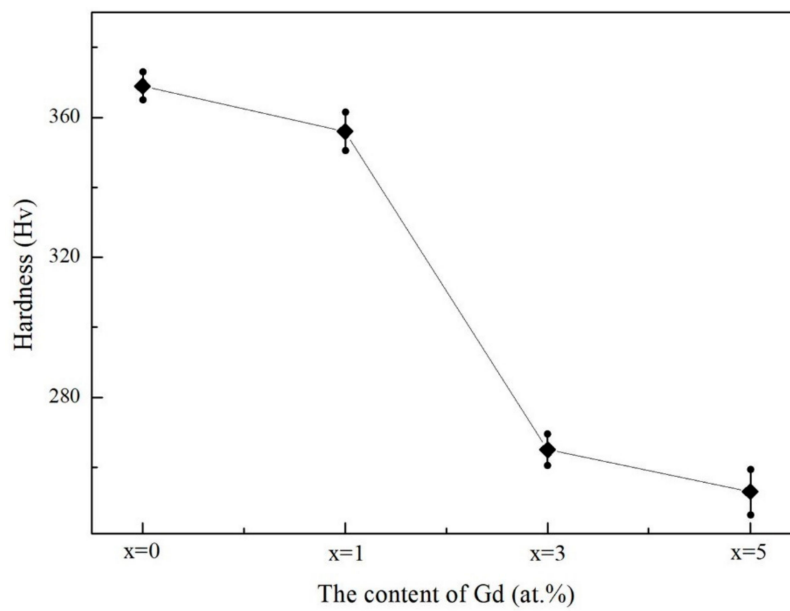


**Figure 5.** The Vickers hardness of the sample with Gd doping.

### 3.2.2. Effect of Ga Doping on Strength and Ductility

The stress-strain curves of the sample with Gd doping were obtained by compression tests and the results are shown in Figure 6. From the stress-strain curves, it can be said that the sample without Gd doping appears to have high yield strength (2274 MPa) and a worst ductility (4.2%). After a small amount of Gd doping ( $x = 1$ ), the yield strength of the sample slightly decreases from 2274 MPa to 2012 MPa, however, the ductility improves from 4.2% to 8.7%. With more Gd doping ( $x = 3$ ), the yield strength further decreases to 1813 MPa and the ductility significantly improves to 10.4%. When the content doping of Gd reaches 5 at.%, the yield strength of the sample decreases to 1630 MPa. The ductility of the sample increases further to 12.9%. It is interesting to note that the strain of sample with 3 and 5 at.% Gd doping shows a very slow growth and represents a platform in the stress-strain curves.

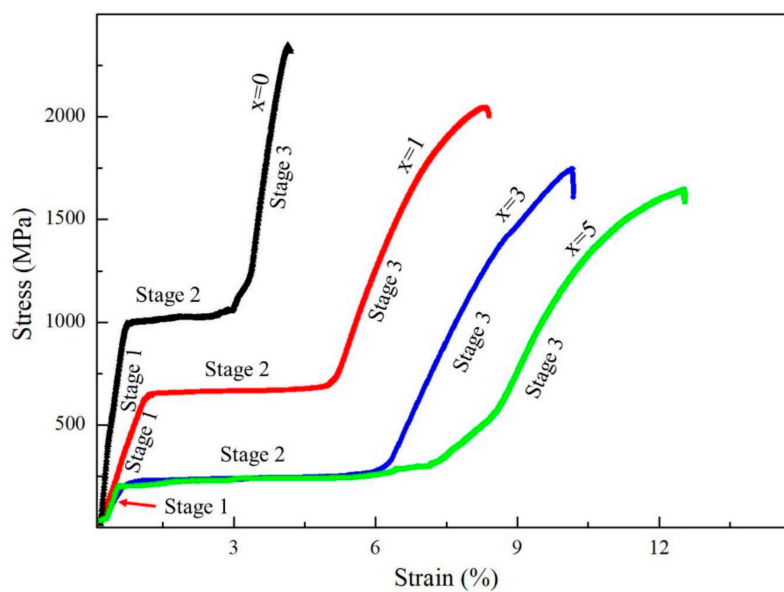


**Figure 6.** The stress-strain curves of the sample with Gd doping by compression tests.

### 3.2.3. Discussions on Mechanical Properties with Ga Doping

It is clear that the influences of Gd doping content on the mechanical properties (i.e., hardness, strength and ductility) are significant. The hardness and strength of the sample appears “snake”-like decreasing tendency, and the ductility appears “snake”-like increasing tendency with the Gd doping content from 0 to 5 at.%. The reason can be ascribed in to two aspects. One is that the increasing volume fraction of  $\gamma$  phases when Gd doping content is increased. As is well known, the  $\gamma$  phase is a kind of soft phase in the Co-Ni-Al system due to their A1 type structure [5]. Figure 7 shows the micro-hardness (load 10 N) of martensite and  $\gamma$  phase of the samples doped with 1 and 3 at.% Gd. It is confirmed that the  $\gamma$  phase (428 HV) is softer than the  $\beta$  phase (632 HV) or martensite (715 HV). Figure 8 shows the volume fraction of  $\gamma$  phases with Gd doping. The volume fraction of  $\gamma$  phases increases with increasing Gd content. Therefore, with increasing the volume fraction of  $\gamma$  phases in alloy, the hardness and strength should be decreases, and the ductility should be increased. Another reason is the stress-induced deformation of twin martensite. The stress-strain curve platforms in Figure 6 ( $x = 3$ ) and ( $x = 5$ ) (a large strain occurred in the sample with in a small range of stress variations) indicate that the twin martensite in the sample was deformed by the stress during hardness and compression test.

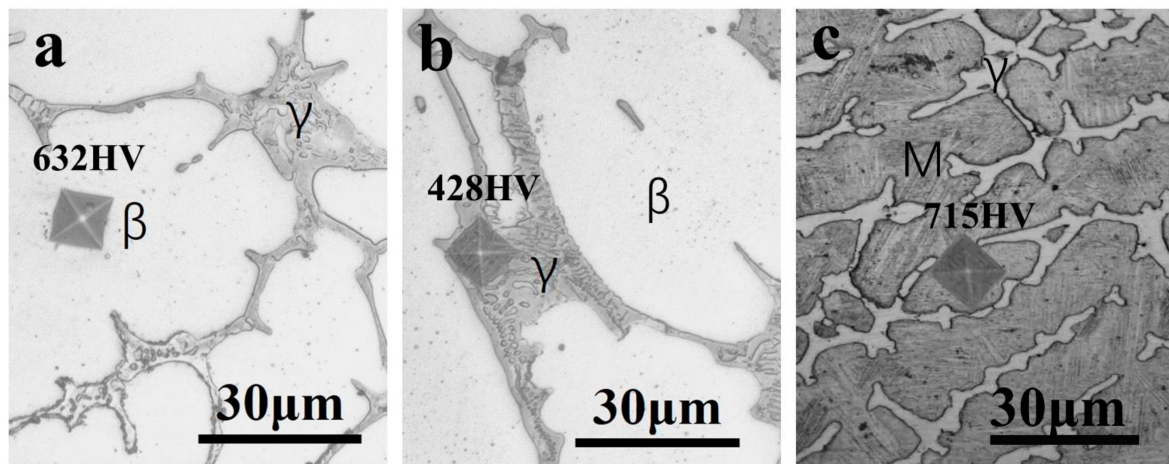


**Figure 7.** The micro-hardness of  $\beta$  phase (a),  $\gamma$  phase (b), and martensite (c) in the sample with 1 and 3 at.% Gd doping.

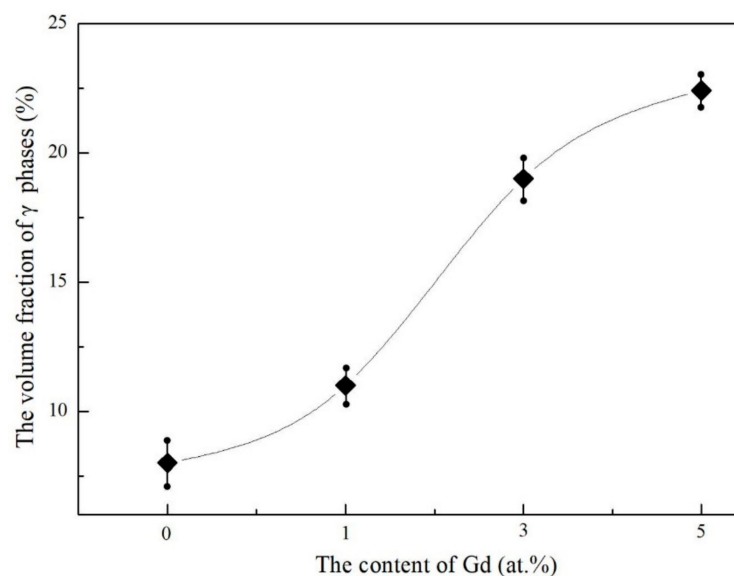


**Figure 8.** The volume fraction of  $\gamma$  phases with Gd doping.

#### 4. Conclusions

In order to improve the mechanical properties and phase transformation temperature, different amount of Gd was doped in  $\text{Co}_{35}\text{Ni}_{32}\text{Al}_{33}$  FSMAs. The influence of Gd doping content on the microstructure variation, phase transformation temperature and mechanical properties of  $\text{Co}_{35}\text{Ni}_{32}\text{Al}_{33}$  alloy was investigated. The main results are given below:

- (1) The microstructure of the shows appeared typical dual-phase structure with Gd doping. The sample with less Gd doping content ( $x = 0$  or  $x = 1$ ) exhibits  $\gamma$  phase and  $\beta$  phase. Whereas, with the Gd doping of 3 and 5 at.%, the microstructure of the sample consists of a  $\gamma$  phase and martensite structure.
- (2) The martensitic transformation process of all samples exhibits one-step thermo-elastic transformation and the martensitic transformation temperature increases apparently with Gd doping. When the Gd content was 3 at.% or more, the phase transformation temperature found to be above room temperature.
- (3) The micro-hardness test of the samples revealed that the  $\gamma$  phase is softer than the  $\beta$  phase and martensite. With Gd doping, more  $\gamma$  phases appeared in the sample that results in the decrease in hardness.
- (4) The sample without Gd doping displays a high yield strength (2274 MPa) and a low ductility of only 4.2%. With the Gd doping, the strength of the sample continuously decreased and the ductility significantly improved. The best ductility of the sample achieved to be 12.9% at the Gd doping content of 5 at.%.

**Author Contributions:** J.J. and L.S. conceived and designed the experiments; H.L. (Huan Liu) and J.J. performed the experiments; C.Y. and Z.L. contributed materials; Y.K. and J.J. analyzed the data; and H.L. (Hong Li). and J.J. wrote the paper. All authors have discussed the results, read and approved the final manuscript.

**Funding:** This research was funded by the Scientific Foundation of Nanjing Institute of Technology (grant number YKJ201504), the Natural Science Foundation of Jiangsu Province of China (grant number BK20181475), School Research Foundation of Nanjing Institute of Technology (grant number CKJA201702), Basic research project of Nanjing Institute of Technology (grant number JCYJ201605), the postdoctoral research selected funding project of Zhejiang province and Outstanding Scientific and Technological Innovation Team in Colleges and Universities of Jiangsu Province.

**Conflicts of Interest:** The authors declare no conflict of interest.

#### References

1. Ullakko, K.; Huang, J.K.; Kantner, C.; O’Handley, R.C.; Kokorin, V.V. Large magnetic-field-induced strains in  $\text{Ni}_2\text{MnGa}$  single crystals. *Appl. Phys. Lett.* **1996**, *69*, 1966. [[CrossRef](#)]
2. Mendonca, A.A.; Jurado, J.F.; Stuard, S.J.; Silva, L.E.L.; Eslava, G.G.; Cohen, L.F.; Ghivelder, L.; Gomes, A.M. Giant magnetic-field-induced strain in  $\text{Ni}_2\text{MnGa}$ -based polycrystal. *J. Alloys Compd.* **2018**, *738*, 509–514. [[CrossRef](#)]
3. Sozinov, A.; Soroka, A.; Lanska, N.; Rames, M.; Straka, L.; Ullakko, K. Temperature dependence of twinning and magnetic stresses in  $\text{Ni}_{46}\text{Mn}_{24}\text{Ga}_{22}\text{Co}_4\text{Cu}_4$  alloy with giant 12% magnetic field-induced strain. *Scr. Mater.* **2017**, *131*, 33–36. [[CrossRef](#)]
4. Lawrence, T.; Lindquist, P.; Ullakko, K.; Mullner, P. Fatigue life and fracture mechanics of unconstrained  $\text{Ni-Mn-Ga}$  single crystals in a rotating magnetic field. *Mater. Sci. Eng. A* **2016**, *654*, 221–227. [[CrossRef](#)]
5. Ju, J.; Yang, L.; Hao, S.; Mao, Q.T.; Lou, S.T.; Liu, H. Microstructure, Martensite Transition and Mechanical Properties Investigations of Polycrystalline  $\text{Co-Ni-Al}$  Alloys with Er Doping. *J. Mater. Eng. Perform.* **2017**, *26*, 1062–1068. [[CrossRef](#)]
6. Yamakov, V.; Hochhalter, J.D.; Leser, W.P.; Warner, J.E.; Newman, J.A.; Pun, G.P.P.; Mishin, Y. Multiscale modeling of sensory properties of  $\text{Co-Ni-Al}$  shape memory particles embedded in an Al metal matrix. *J. Mater. Sci.* **2016**, *51*, 1204–1216. [[CrossRef](#)]
7. Rekik, H.; Krifa, M.; Bachaga, T.; Escoda, L.; Sunol, J.J.; Khitouni, M.; Chmingue, M. Structural and martensitic transformation of  $\text{MnNiSn}$  shape memory alloys. *Int. J. Adv. Manuf. Technol.* **2017**, *90*, 291–298. [[CrossRef](#)]

8. Sumida, K.; Shirai, K.; Zhu, S.; Taniguchi, M.; Ye, M.; Ueda, S.; Takeda, Y.; Saitoh, Y.; Aseguinolaza, I.R.; Barandiarán, J.M.; et al. Spectroscopic evidence of band Jahn-Teller distortion upon martensitic phase transition in Heusler-type Ni-Fe(Co)-Ga ferromagnetic shape-memory alloy films. *Phys. Rev. B* **2015**, *91*. [[CrossRef](#)]
9. Wang, Y.; Huang, C.H.; Wu, H.J.; Liao, X.Q.; Gao, J.H.; Wang, D.; Yang, S.; Song, X. Effect of martensitic structure on the magnetic field controlled damping effect in a Ni-Fe-Mn-Ga ferromagnetic shape memory alloy. *J. Mater. Sci.* **2017**, *52*, 12854–12860. [[CrossRef](#)]
10. Dye, D. Shape Memory Alloys Towards practical actuators. *Nat. Mater.* **2015**, *14*, 760–761. [[CrossRef](#)] [[PubMed](#)]
11. Ju, J.; Lou, S.T.; Yang, L.; Li, T.; Hao, S.; Yan, C. Effect of Electronic and Magnetic Valences on Phase Transition and Magnetic Properties in Co-Ni-Al-RE (RE = Gd, Dy and Er) Alloys. *J. Electron. Mater.* **2017**, *46*, 1390–1395. [[CrossRef](#)]
12. Seiner, H.; Kopecek, J.; Sedlak, P.; Bodnarova, L.; Landa, M.; Sedmak, P.; Heczko, O. Microstructure, martensitic transformation and anomalies in  $c'$ -softening in Co-Ni-Al ferromagnetic shape memory alloys. *Acta Mater.* **2013**, *61*, 5869–5876. [[CrossRef](#)]
13. Heczko, O.; Seiner, H.; Sedlak, P.; Kopecek, J.; Kopecky, V.; Landa, M. Resonant ultrasound spectroscopy—A tool to probe magneto-elastic properties of ferromagnetic shape memory alloys. *Eur. Phys. J. B* **2013**, *86*, 62. [[CrossRef](#)]
14. Titenko, A.N. Martensitic Transformations in Ferromagnetic Co-Ni-Al Alloy with Shape Memory Caused by Uniaxial Stretching. *Metall. Noveishie Tekhnol.* **2012**, *34*, 843–854.
15. Scheerbaum, N.; Kraus, R.; Liu, J.; Skrotzki, W.; Schultz, L.; Gutfleisch, O. Reproducibility of martensitic transformation and phase constitution in Ni-Co-Al. *Intermetallics* **2012**, *20*, 55–62. [[CrossRef](#)]
16. Ju, J.; Xue, F.; Zhou, J.; Bai, J.; Sun, L.X. Microstructure and mechanical properties change by rare earth Dy added in as-cast Co-Ni-Al ferromagnetic shape memory alloys. *Mater. Sci. Eng. A* **2014**, *616*, 196–200. [[CrossRef](#)]
17. Li, P.Z.; Karaca, H.E.; Chumlyakov, Y.I. Orientation dependent compression behavior of Co<sub>35</sub>Ni<sub>35</sub>Al<sub>30</sub> single crystals. *J. Alloys Compd.* **2017**, *718*, 326–334. [[CrossRef](#)]
18. Barriobero-Vila, P.; Gussone, J.; Stark, A.; Schell, N.; Haubrich, J.; Requena, G. Peritectic titanium alloys for 3D printing. *Nat. Commun.* **2018**, *9*. [[CrossRef](#)] [[PubMed](#)]
19. Barriobero-Vila, P.; Oliveira, V.B.; Schwarz, S.; Buslaps, T.; Requena, G. Tracking the alpha martensite decomposition during continuous heating of a Ti-6Al-6V-2Sn alloy. *Acta Mater.* **2017**, *135*, 132–143. [[CrossRef](#)]
20. Barriobero-Vila, P.; Requena, G.; Warchomicka, F.; Stark, A.; Schell, N.; Buslaps, T. Phase transformation kinetics during continuous heating of a beta-quenched Ti-10V-2Fe-3Al alloy. *J. Mater. Sci.* **2015**, *50*, 1412–1426. [[CrossRef](#)]
21. Kurnsteiner, P.; Wilms, M.B.; Weisheit, A.; Barriobero-Vila, P.; Jagle, E.A.; Raabe, D. Massive nanoprecipitation in an Fe-19Ni-xAl maraging steel triggered by the intrinsic heat treatment during laser metal deposition. *Acta Mater.* **2017**, *129*, 52–60. [[CrossRef](#)]
22. Ju, J.; Xue, F.; Li, H. Microstructure and Magnetic Property Variation with Addition of Rare Earth Element Dy in Co-Ni-Al Ferromagnetic Shape Memory Alloy. *J. Iron Steel Res. Int.* **2015**, *22*, 858–863. [[CrossRef](#)]
23. Zhao, Z.Q.; Wu, S.X.; Wang, F.S.; Wang, Q.; Jiang, L.P.; Wang, X.L. Large magnetic-field-induced strains in rare earth polycrystalline Ni-Mn-Ga. *Rare Met.* **2004**, *23*, 241–245.
24. Tsuchiya, K.; Tsutsumi, A.; Ohtsuka, H.; Umemoto, M. Modification of Ni-Mn-Ga ferromagnetic shape memory alloy by addition of rare earth elements. *Mater. Sci. Eng. A* **2004**, *378*, 370–376. [[CrossRef](#)]
25. Fan, Z.Y.; Shi, J.W.; Gao, C.; Gao, G.; Wang, B.R.; Wang, Y.; He, C.; Niu, C. Gd-modified MnO<sub>x</sub> for the selective catalytic reduction of NO by NH<sub>3</sub>: The promoting effect of Gd on the catalytic performance and sulfur resistance. *Chem. Eng. J.* **2018**, *348*, 820–830. [[CrossRef](#)]
26. Franco, A.; Banerjee, P.; Romanholo, P.L. Effect of composition induced transition in the optical band-gap, dielectric and magnetic properties of Gd doped Na<sub>0.5</sub>Bi<sub>0.5</sub>TiO<sub>3</sub> complex perovskite. *J. Alloys Compd.* **2018**, *764*, 122–127. [[CrossRef](#)]

